Structure of Nanocrystalline Alkali Metal Manganese Oxides by the Atomic Pair Distribution Function Technique

Milen Gateshki,[†] Seong-Ju Hwang,[‡] Dae Hoon Park,[‡] Yang Ren,[§] and Valeri Petkov*[,†]

Department of Physics, Central Michigan University, 203 Dow Science, Mt. Pleasant, Michigan 48859, Department of Applied Chemistry and Center for Emerging Wireless Transmission Technology, College of Natural Sciences, Konkuk University, Chungju Campus, Chungbuk 380-701, Korea, and Advanced Photon Source, Argonne National Laboratory, Argonne, Illinois 60439

Received: April 15, 2004

The atomic scale structures of two nanocrystalline K−Li−Mn−O−I materials obtained through *Chimie Douce* route in aqueous and acetone solutions have been determined using X-ray diffraction and atomic Pair Distribution Function technique. Both samples have been found to possess a layered-type structure, where the layers are made of edge-shared MnO_6 octahedra. With the sample prepared in aqueous solution, the layers are well separated and the interlayer space is occupied by both Li and K atoms. With the sample prepared in acetone solution the Mn−O layers are not so well separated and encapsulate mostly Li atoms. This material exhibits some Li/Mn substitutional disorder as well. The new structural information has been used to explain the electrochemical behavior of the two nanocrystalline materials. Some methodological aspects of the atomic pair distribution function technique and its applicability to study the structure of crystalline and nanocrystalline materials have been discussed as well.

Introduction

Recently, lithium manganese oxides have been extensively studied due to their potential use as cathode materials in Li ion batteries.[1] The main advantage of the manganese based cathode materials over the widely used $LiCoO_2$ is that manganese is nontoxic and relatively cheap. The studies have led to the discovery of a number of lithium manganese oxides with different stoichiometries, crystal structures, and electrochemical properties. Among them, cubic spinel $LiMn_2O_4$, tetragonal spinel $Li_2Mn_2O_4$, orthorhombic $LiMnO_2$, layered monoclinic Li_2MnO_3, and $LiMnO_2$ have attracted special attention as promising candidates.[2−10] Despite the demonstrated structural and chemical flexibility and many obvious advantages, crystalline lithium manganese oxides have not found a widespread application due to their structural instability. It has been reported that most of lithium manganates rapidly transform to a material with spinel-type structure and lose their useful properties during the electrochemical charge−discharge cycle. Work toward solving the problem has resulted in the development of a new class of nanocrystalline lithium manganese oxides with better structural stability, larger capacity, and smoother discharge curves.[11−14] Understanding the improved performance of the nanocrystalline materials requires a good knowledge of their atomic ordering and that is why several studies have been carried out by employing structure-sensitive techniques such as Raman and X-ray absorption spectroscopy (XAS).[11,14] However, no complete 3D structure determination has been done so far. The reason is that nanocrystalline materials show diffraction patterns with a very few, if any, Bragg peaks and a pronounced diffuse component rendering conventional crystallography inapplicable. In this paper, we describe a determination of the atomic scale structure of two nanocrystalline lithium manganese oxides by the nontraditional Atomic Pair Distribution Function (PDF) technique. It has emerged recently as a powerful tool for structural characterization of materials of limited structural coherence including nanocrystals.[15,16] The strength of the technique comes from the fact that it takes all components of the diffraction data (Bragg peaks and diffuse scattering) into account and thus reveals both the longer range atomic order and the local deviations from it. In contrast, techniques employed to study crystalline materials (e.g., Rietveld method[17,18]) rely only on Bragg peaks in the diffraction data and are not so sensitive to the local structural imperfections in materials. Here we show that both nanocrystalline lithium manganese oxides studied have a layered structure that is very well defined on the nanometer length scale and may well be described with a small number of parameters, such as unit cell and symmetry. Our PDF studies also reveal other important structural details in the nanocrystalline materials such as the interlayer distance and the type of atomic species encapsulated between the layers. The new structural information reported here well explains material's properties facilitating further progress in Li batteries research.

Experimental Section

Sample Preparation. Two different nanocrystalline lithium manganese oxides were studied in the present work: one obtained via aqueous and the other via nonaqueous route. Respectively, they were prepared by reacting water and acetone solutions of $KMnO_4$ with 1.5 equiv of LiI at room temperature, similarly to the previously reported *Chimie Douce* method.[11,19,20] The mixed solutions were maintained for 1 day under constant stirring. The resulting precipitates were washed with water for the water-based sample, and acetone and methanol for the acetone-based sample. Then the samples were dried at 130 °C

* To whom all correspondence should be addressed. E-mail: petkov@phy.cmich.edu.
[†] Central Michigan University.
[‡] Konkuk University.
[§] Argonne National Laboratory.

10.1021/jp048340k CCC: $27.50
Published on Web 09/03/2004

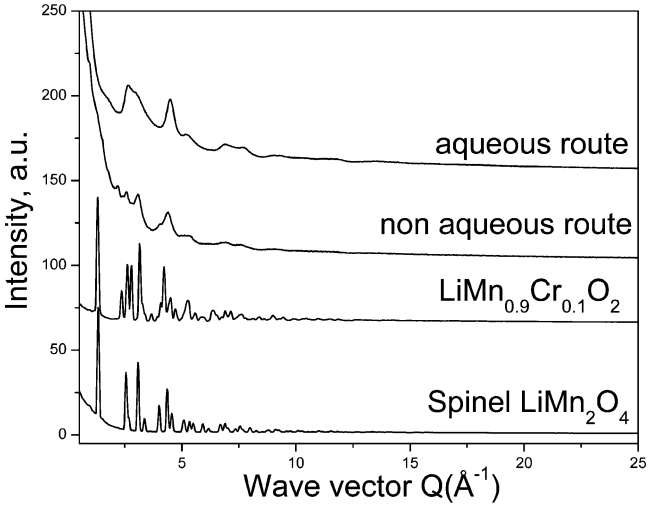

Figure 1. Experimental powder diffraction spectra for crystalline $LiMn_{0.9}Cr_{0.1}O_2$, $LiMn_2O_4$, and nanocrystalline lithium manganese oxides obtained through aqueous and nonaqueous routes.

(80 °C for the water-based sample) in a vacuum. The chemical compositions of the samples were determined by atomic absorption (AA) spectrometry, inductive coupled plasma (ICP) spectrometry, thermogravimetric analysis (TGA), and electron probe microanalysis (EPMA). The chemical compositions of the nanocrystals were found to be $Li_{0.54}K_{0.31}MnO_{3.0-\delta}I_{0.10}$ for the water-based sample and $Li_{1.28}K_{0.36}MnO_{3.0-\delta}I_{0.03}$ for the acetone-based sample, respectively. Due to its relatively small concentration, iodine was not explicitly taken into account in the structure determination studies. TGA results showed that the water-based sample contains about 0.2 mol of water per unit formula. Due to their weak scattering power, water species were not taken into account either. However, as the results of our studies show, water plays a certain role in determining important features in the atomic-scale structure and thus has an impact on the electrochemical properties of the nanocrystalline materials studied.

In addition to the nanocrystalline samples, we prepared and studied two crystalline lithium manganese oxides: $LiMn_{0.9}Cr_{0.1}O_2$ and $LiMn_2O_4$. The former was prepared by heating a stoichiometric mixture of Li_2CO_3, Mn_2O_3, and Cr_2O_3 at 940 °C under argon flow to suppress the oxidation of manganese. The latter was also prepared by a conventional solid-state reaction involving heating Li_2CO_3 and Mn_2O_3 in ambient atmosphere at 830 °C. All four samples studied, two crystalline and two nanocrystalline, were carefully packed between Kapton foils to avoid texture formation and subject to diffraction experiments.

Synchrotron Radiation Diffraction Experiments. X-ray diffraction experiments were carried out at the beamline 11-ID-C (Advanced Photon Source, Argonne National Laboratory) using X-rays of energy 115.013 keV ($\lambda = 0.1078$ Å). The higher energy X-rays were used to extend the region of reciprocal space covered (i.e. to obtain data at higher wave vectors, Q), which is important for the success of PDF analysis. The measurements were carried out in symmetric transmission geometry and scattered radiation was collected with an intrinsic germanium detector connected to a multichannel analyzer. Several runs were conducted with each of the samples and the resulting XRD patterns averaged to improve the statistical accuracy and reduce any systematic effect due to instabilities in the experimental setup. The diffraction patterns obtained are shown in Figure 1. As can be seen, the XRD patterns of $LiMn_{0.9}Cr_{0.1}O_2$ and $LiMn_2O_4$ exhibit well-defined Bragg peaks up to $Q \approx 13-15$ Å^{-1}. These materials are obviously perfectly crystalline solids. The XRD patterns of the two nanocrystalline materials, on the other hand, contain a few Bragg-like features and a pronounced diffuse component. Such diffraction patterns are practically impossible to tackle by ordinary techniques for structure determination. However, once reduced to the corresponding atomic PDFs, they become a structure-sensitive quantity lending itself to structure determination.

The frequently used reduced atomic PDF, $G(r)$, is defined as follows:

$$G(r) = 4\pi r[\rho(r) - \rho_0] \quad (1)$$

where $\rho(r)$ and ρ_0 are the local and average atomic number densities, respectively, and r is the radial distance. It peaks at characteristic distances separating pairs of atoms and thus reflects the atomic structure. The PDF $G(r)$ is the Fourier transform of the experimentally observable total structure function, $S(Q)$, i.e.,

$$G(r) = (2/\pi)\int_{Q=0}^{Q_{max}} Q[S(Q) - 1]\sin(Qr)\,dQ \quad (2)$$

where Q is the magnitude of the wave vector $Q = (4\pi \sin\theta)/\lambda$, 2θ is the angle between the incoming and outgoing radiation beams, and λ is the wavelength of the radiation used. The structure function is related to the coherent part of the total diffracted intensity of the material as follows:

$$S(Q) = 1 + [I^{coh}(Q) - \sum c_i|f_i(Q)|^2]/|\sum c_i f_i(Q)|^2 \quad (3)$$

where $I^{coh}(Q)$is the coherent scattering intensity per atom in electron units and c_i and f_i are the atomic concentration and X-ray scattering factor, respectively, for the atomic species of type i.[21,22] As can be seen from eqs 1−3, $G(r)$ is simply another representation of the powder diffraction data. However, exploring the diffraction data in real space is advantageous, especially in the case of materials with limited structural coherence. First, eq 2 implies that the *total* scattering, including Bragg scattering as well as diffuse scattering, contributes to the PDF. In this way both the longer range atomic structure, manifested in the sharp Bragg peaks, and the local nonperiodic structural imperfections, manifested in the diffuse components of the diffraction pattern, are reflected in the PDF. Second, by accessing high values of Q, experimental $G(r)$ functions with high real-space resolution can be obtained and hence, quite fine structural features can be revealed.[23] In fact, data at high Q values ($Q >$ 15 Å^{-1}) are critical to the success of PDF analysis. Third, $G(r)$ is less affected by diffraction optics and experimental factors since these are accounted for in the step of extracting the coherent intensities from the raw diffraction data. This renders the PDF a structure-dependent quantity that gives directly relative positions of atoms in materials. As demonstrated here, this enables convenient testing and refinement of structural models.

Experimental PDFs for the studied samples were obtained as follows. First, the coherently scattered intensities were extracted from the XRD patterns of Figure 1 by applying appropriate corrections for flux, background, Compton scattering, and sample absorption. The intensities were normalized in absolute electron units, reduced to structure functions $Q[S(Q) - 1]$, and Fourier transformed to atomic PDFs. All data processing was done with the program RAD.[24] Thus obtained experimental PDFs are shown in Figure 2. As can be seen, the experimental PDFs for crystalline $LiMn_{0.9}Cr_{0.1}O_2$ and $LiMn_2O_4$ are rich in well-defined structural features extending to very high real-

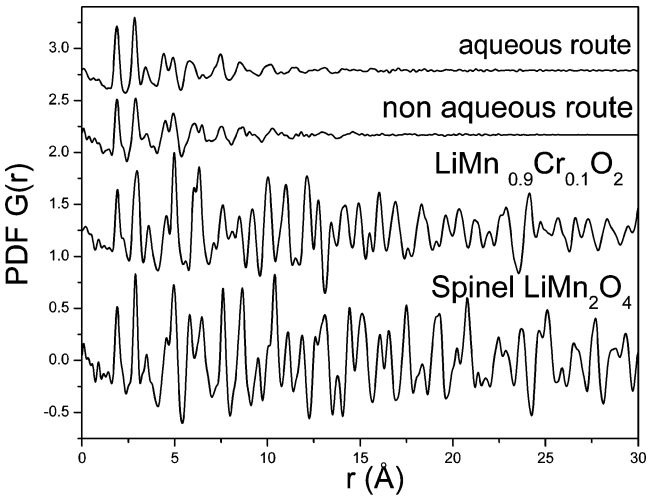

Figure 2. Atomic PDFs obtained from the diffraction data of Figure 1.

space distances, as it should be with materials possessing 3D periodicity and long-range atomic order. The PDFs for the nanocrystalline materials are also rich in well-defined features but those features vanish already at 15 Å. Obviously, the nanocrystalline samples have a very well-defined local atomic arrangement but lack the extended order of usual crystals.

Results and Discussion

Crystalline Samples. Even though the structures of crystalline $LiMn_{0.9}Cr_{0.1}O_2$ and $LiMn_2O_4$ are well-known, they were again studied here to test the quality of the present experiments and demonstrate the capabilities of the PDF technique. The crystalline $LiMn_2O_4$ possesses a cubic spinel-type structure built of perfect MnO_6 octahedral units organized in a 3D network with Li atoms occupying open channels in it. The crystalline $LiMn_{0.9}Cr_{0.1}O_2$ may be viewed as a stack of layers consisting of edge-shared Mn(or Cr)O_6 octahedral units with Li atoms occupying the interlayer octahedral sites. Fragments of both structures are shown in Figure 3, parts a and g, respectively.

The structures of both crystalline materials were first approached with conventional crystallographic techniques such as the Rietveld method.[17,18] It is a well-established technique for crystal structure determination and refinement from powder diffraction data. The method employs a least-squares procedure to compare experimental and model powder diffraction patterns calculated from a plausible structural model. The structural parameters of the model are adjusted until the best fit to the experimental diffraction data is achieved. The progress of the fit is assessed by computing various agreement factors with the most frequently used being[18]

$$R_{\mathrm{wp}} = \left\{ \frac{\sum w_i (y_i^{\mathrm{obs}} - y_i^{\mathrm{calc}})^2}{\sum w_i (y_i^{\mathrm{obs}})^2} \right\}^{1/2} \qquad (4)$$

here y_i^{obs} and y_i^{calc} are the observed and calculated data points and w_i are weighting factors taking into account the statistical accuracy of the diffraction experiment. The Rietveld method has been implemented in a number of user-friendly computer programs, such as RIETAN[25] and GSAS.[26] Here we used the program FullProf.[27]

Experimental diffraction data for $LiMn_2O_4$ and $LiMn_{0.9}Cr_{0.1}O_2$ are shown in Figure 4, parts a and b, respectively, together with the best model data resulting from Rietveld refinements. Structure data from literature sources[28,29] were used as initial values for the refinable parameters. Note that the presence of a small amount of Cr in $LiMn_{0.9}Cr_{0.1}O_2$ was not explicitly taken into account in the present refinements; rather the sample was considered to have a nominal composition "$LiMnO_2$", which is a reasonable approximation given the similar X-ray scattering factors of Mn and Cr. In the case of $LiMn_2O_4$, the lattice constant a, the atomic position of oxygen, and the thermal factors of Mn, Li, and oxygen atoms were refined. With $LiMn_{0.9}Cr_{0.1}O_2$ the three lattice constants, the monoclinic angle β, the atomic position of oxygen atoms, and the thermal factors of Mn, Li, and oxygen atoms were refined against the experimental diffraction data. The refined values of the structural parameters for $LiMn_2O_4$ and $LiMn_{0.9}Cr_{0.1}O_2$ are summarized in Tables 1 and 2, respectively. They are consistent with previous results and well account for all Bragg peaks in the diffraction data, including the low intensity ones at higher 2θ values (see the insets in Figure 4a,b). Next, the same structure models were fit to the corresponding experimental PDFs. Again, the presence of a small amount of Cr in layered $LiMn_{0.9}Cr_{0.1}O_2$ was not taken into account. The fit was done with the help of the program PDFFIT[30] and was constrained to have the symmetry of the respective structure models. An agreement factor, R_G, defined as

$$R_{\mathrm{G}} = \left\{ \frac{\sum w_i (G_i^{\mathrm{exp}} - G_i^{\mathrm{calc}})^2}{\sum w_i (G_i^{\mathrm{exp}})^2} \right\}^{1/2} \qquad (5)$$

was used to estimate the progress of the structure refinement. Here, G^{exp} and G^{calc} are the experimental and calculated PDF data, respectively, and w_i are weighting factors reflecting the statistical quality of the experimental data. The best fits achieved for $LiMn_{0.9}Cr_{0.1}O_2$ and $LiMn_2O_4$ are shown in Figure 4, parts c and d, respectively. The level of agreement between the model and experimental PDF data is fairly good. The refined structural parameters are again summarized in Tables 1 and 2.

TABLE 1: Structural Parameters for $LiMn_2O_4$ As Obtained through Rietveld and PDF Methods

parameter	Rietveld	PDF
a, Å	8.265(2)	8.252(1)
x(O)[a]	0.3873(2)	0.3873(4)
B(Mn), Å^2	0.57(1)	0.85(1)
B(Li), Å^2	1.4(3)	4.1(1)
B(O), Å^2	1.28(7)	2.84(8)
R_{wp}(R_{G}), %	10.2	16.6

[a] The three atoms in the asymmetric unit occupy the following Wyckoff positions: Mn 16d(5/8,5/8,5/8); Li 8a(0,0,0); O 32e(x,x,x). Atomic positions are refined in the space group $Fd\bar{3}m$.

TABLE 2: Structural Parameters for $LiMn_{0.9}Cr_{0.1}O_2$ As Obtained through Rietveld and PDF Methods

parameter	Rietveld	PDF
a, Å	5.409(2)	5.414(1)
b, Å	2.820(1)	2.823(1)
c, Å	5.372(2)	5.361(1)
β, deg	115.44(1)	115.44(1)
x(O)[a]	0.265(1)	0.262(1)
z(O)	0.768(1)	0.770(1)
B(Mn/Cr), Å^2	0.49(1)	0.54(1)
B(Li), Å^2	0.2(2)	1.03(1)
B(O), Å^2	0.73(6)	1.17(1)
R_{wp}(R_{G}), %	10.6	22.4

[a] The three atoms in the asymmetric unit occupy the following Wyckoff positions: Mn/Cr 2a(0,0,0); Li 2d(0,$^1/_2$,$^1/_2$); O 4i(x,0,z). Atomic positions are refined in the space group $C2/m$.

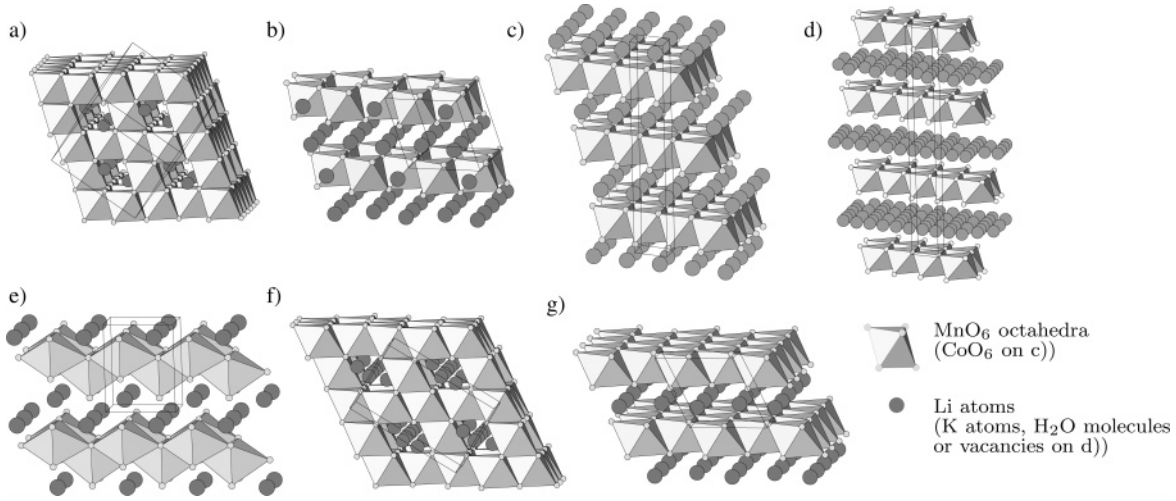

Figure 3. Crystal structures considered as trial models in the structural determination of nanocrystalline lithium manganese oxides: (a) cubic spinel (space group $Fd\bar{3}m$) $LiMn_2O_4$ structure featuring a 3D network of MnO_6 octahedra with Li atoms occupying channels in the network; (b) monoclinic (space group $C2/m$) Li_2MnO_3 structure featuring layers of MnO_6 octahedra with Li atoms encapsulated between the layers as well as occupying one-third of the octahedral sites in the layers; (c) rhombohedral (space group $R\bar{3}m$) O3 type structure, typical for $LiCoO_2$, featuring layers of CoO_6 octahedra encapsulating Li atoms; (d) rhombohedral (space group $R\bar{3}m$) $K_xMnO_2{\cdot}yH_2O$ structure featuring layers of MnO_6 octahedra encapsulating K atoms and H_2O molecules; (e) orthorhombic (space group $Pmnm$) $LiMnO_2$ structure featuring buckled layers of MnO_6 octahedra encapsulating Li atoms; (f) tetragonal (space group $I4_1/amd$) $Li_2Mn_2O_4$ which may be considered as a distorted spinel structure; (g) monoclinic (space group $C2/m$) layered $LiMnO_2$ structure with Jahn−Teller distorted MnO_6 octahedra.

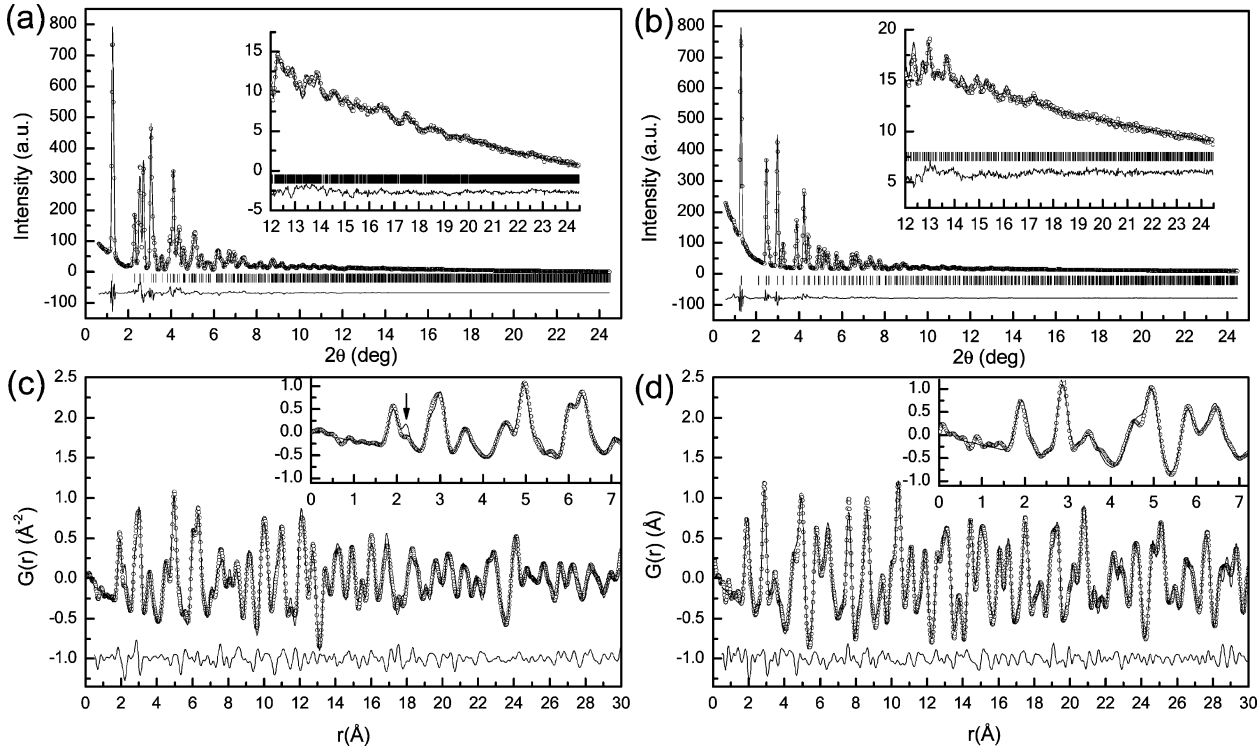

Figure 4. Plots a and b show Rietveld refinements of the powder diffraction patterns ($\lambda = 0.1078$ Å) of $LiMn_{0.9}Cr_{0.1}O_2$ and $LiMn_2O_4$, respectively. Plot c shows the refinement of the PDF of $LiMn_{0.9}Cr_{0.1}O_2$, and plot d shows that of $LiMn_2O_4$. On the four plots, dots represent experimental data and lines represent calculated and difference profiles (given in the lower part of the plots). The arrow in the inset in plot c points to the position of longer Mn−O bonds in Jahn−Teller distorted octahedra. The corresponding PDF peak in the experimental data is of amplitude lower than that predicted for a complete Jahn−Teller distortion of the material. This is to be expected since the Jahn−Teller distortion in $LiMn_{0.9}Cr_{0.1}O_2$ is reduced due to the partial substitution of Mn by Cr.

A comparison between the structural parameters such as lattice constants and atomic positions resulting from the Rietveld and PDF fits shows that both techniques yield very similar results in the case of crystalline materials. In particular, both methods confirm that the $LiMn_2O_4$ sample has a cubic (space group $Fd\bar{3}m$) spinel-like structure and that $LiMn_{0.9}Cr_{0.1}O_2$ has a monoclinically distorted (space group $C2/m$) O3-type layered structure. The two techniques, however, yield somewhat different thermal factors for the light atomic species: Li and O. Possible reasons for a discrepancy of this type have been discussed in a recent paper.[31]

Also, it is worth noting that the agreement factor R_G (see eq 5) achieved with the PDF-based refinement appears higher when compared to the corresponding R_{wp} factor (eq 4) achieved in the Rietveld refinements (see Tables 1 and 2). This does not indicate that the PDF guided fit is of inferior quality since it

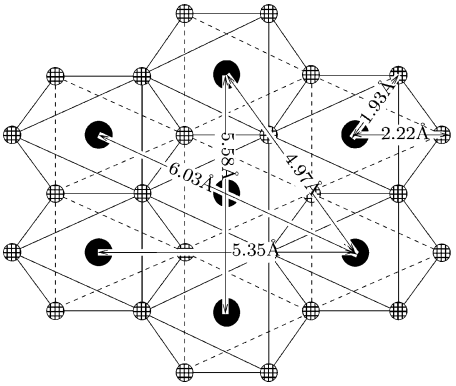

Figure 5. Top view of the MnO_2 layer in monoclinic, Jahn−Teller distorted $LiMnO_2$. Black circles represent Mn atoms, and hatched circles represent O atoms. The distances shown are calculated from the atomic positions refined in the present study.

yields structural parameters that agree quite well with those obtained by the Rietveld method. Rather, it reflects the fact that the experimental quantities being fit in real and reciprocal space are not the same. This outcome of our study shows that the inherently higher absolute value of the agreement factor used in PDF-based refinements does not affect its functional purpose as a residual function that must be minimized to find the best fit and as a quantity allowing the differentiation between competing structural models.

The performance of the two techniques is, however, substantially different when the material shows some intrinsic disorder as is the case with $LiMn_{0.9}Cr_{0.1}O_2$. Manganese−oxygen octahedra in monoclinic $LiMnO_2$ are distorted due to the Jahn−Teller effect and show short (∼1.93 Å) and long (∼2.22 Å) Mn−O bonds as illustrated in Figure 5. The presence of Mn−O bonds of different length is well seen in the corresponding PDF having a split first peak with subcomponents located at 1.9 and 2.2 Å (see Figure 4c). The first peak in the PDF for the $LiMn_2O_4$ spinel is not split (see Figure 4d) since MnO_6 octahedra are not distorted in this material. When a fraction of Mn is replaced by Cr, as it is in the sample we studied, the number of octahedral units with Jahn−Teller distortion is seen to diminish (see the inset in Figure 4c). This observation is fully consistent with the finding of previous studies[29] suggesting that when Cr enters the octahedral sites of the transition metal oxide layer, the Jahn−Teller distortion at those sites is quenched. The result shows that the atomic PDF is sensitive to both the presence and the magnitude of local structural distortions and may be confidently employed to study them when present in materials. This is not so easily achieved when the experimental diffraction data are considered in reciprocal space alone.

Nanocrystalline Samples. As can be seen in Figure 1, diffraction patterns of nanocrystalline lithium manganese oxides do not show sharp Bragg peaks and may not be tackled by conventional crystallographic techniques such as the Rietveld method. That is why we approached the diffraction data in real space in terms of the corresponding atomic PDFs. They are shown in Figure 2 (see also Figures 6 and 7). The two experimental PDFs appear quite similar to each other suggesting that the two nanocrystalline materials studied share common structural features. To determine those features we adopted the following procedure: At first, plausible structural models that are consistent with the experimental PDF data and all available structural information for the materials under study were looked for. The models were matched against the experimental data to identify the most promising one. Then, the 3D structure of the nanocrystals was determined through refining that model so that

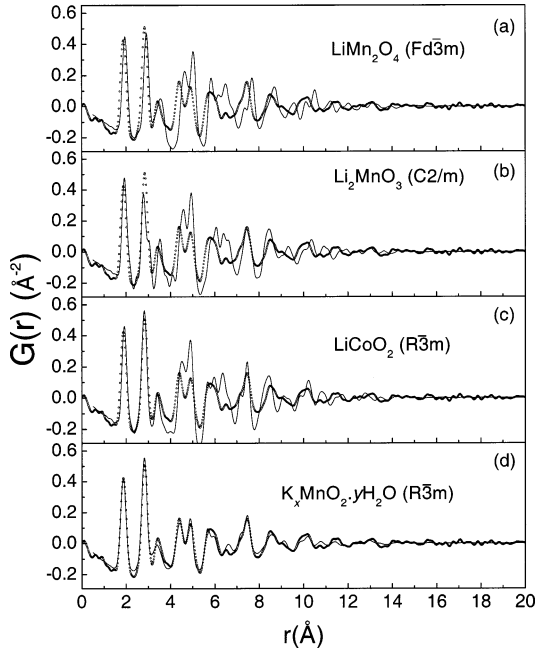

Figure 6. Experimental PDF for the hydrous K−Li−Mn−O−I sample (dots) compared to the calculated PDFs for different structural models.

it reproduces well all important details in the experimental PDF data. The success of this approach has already been demonstrated in several studies on nanocrystals such as $LiMoS_2$,[15] $V_2O_5 \cdot nH_2O$ nanoribbons,[16] and V_2O_5 nanotubes.[32]

A careful inspection of the most prominent features in the experimental PDFs revealed the following structural characteristics of the studied nanocrystals: The first peak in the experimental PDF data is positioned at 1.89 Å. Since this is the typical Mn−O distance in materials with octahedral oxygen coordination around the manganese atoms, we concluded that both nanocrystalline lithium manganese oxides should contain MnO_6 octahedra. For comparison, the Mn−O distance within tetrahedral MnO_4 units is about 1.66 Å. Our PDF data rule out the presence of any such units in the samples. The second PDF peak appears at 2.88 Å, which is the typical Mn−Mn distance for edge-shared MnO_6 octahedra. Thus, the analysis of the experimental PDF data suggested that both nanocrystalline samples are likely to be built of edge-shared MnO_6 octahedra. A similar conclusion has been drawn[12] from micro-Raman and Mn K-edge XANES measurements. Accordingly, we narrowed our search to structures based on edge-shared MnO_6 octahedra only. Several such structures are known to occur with crystalline manganese oxides of chemical composition similar to that of the nanocrystals we study. For the nanocrystalline sample obtained via aqueous route we explored them in turn starting with the structure type found with crystalline $LiMn_2O_4$. That structure features a three-dimensional network of edge-shared MnO_6 octahedra as shown in Figure 3a. As can be seen in Figure 6a, this model reproduces well only the first two peaks in the experimental PDF data but completely fails at longer real-space distances. Obviously, the structure of the nanocrystal is not a 3D network of edge-shared MnO_6 octahedra. Next, a structure type found in Li_2MnO_3 was attempted. The structure features layers of edge-shared octahedral units where two-thirds of the octahedral sites are occupied by Mn atoms and one-third by Li atoms. Mn and Li atoms in the layers are ordered in such a way that each MnO_6 octahedron shares its edges with three other MnO_6 octahedra and three LiO_6 octahedra. A fragment of this structure is shown in Figure 3b. The model did not perform much better, as the results in Figure 6b show, and was not

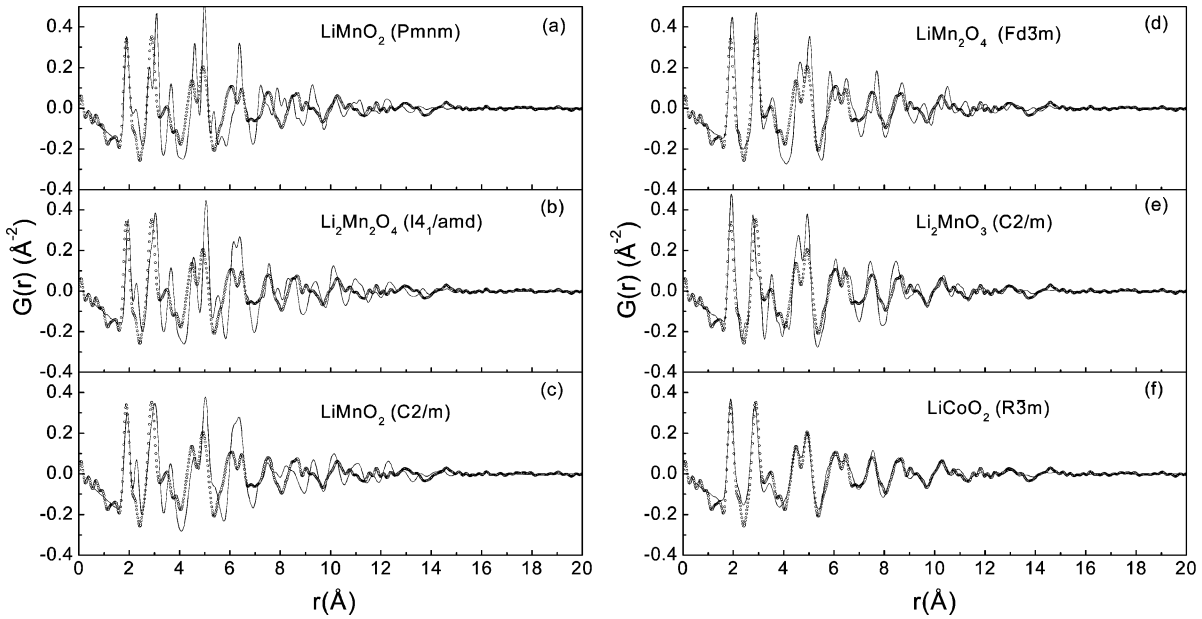

Figure 7. Experimental PDF for the anhydrous K−Li−Mn−O−I sample (dots) compared with calculated PDFs for different structural models. The model PDF data shown in panel f are calculated from a structure model featuring (Li/Mn) disorder as explained in the text.

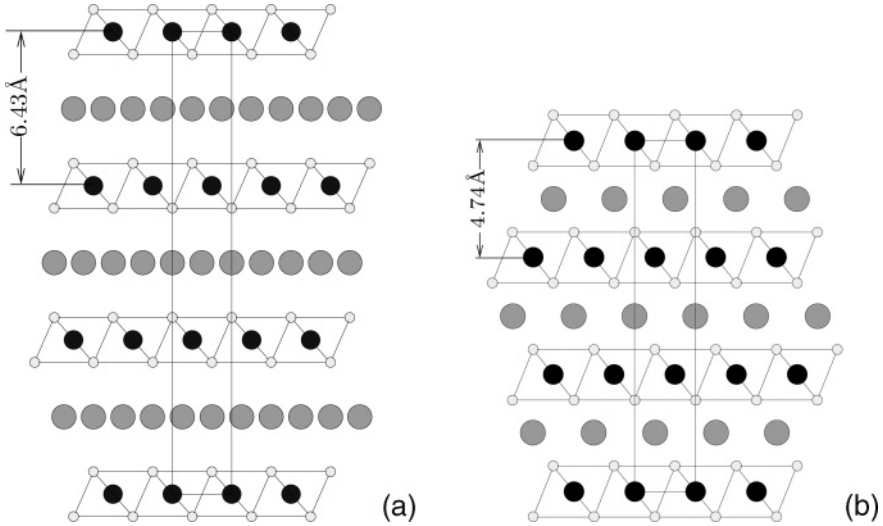

Figure 8. Schematic representations of the structure of the hydrous (a) and anhydrous (b) nanocrystalline K−Li−Mn−O−I samples as obtained by the present PDF studies. Black circles represent Mn atoms, small white circles represent O atoms on the vertexes of octahedral units. In part a, gray circles represent the positions of interlayer K atoms, Li atoms, and residual H_2O molecules; in part b, gray circles represent the positions of interlayer Li atoms and Mn atoms. The interlayer distances are calculated from the refined lattice constants.

pursued further. A model based on the structure type occurring with $LiCoO_2$ was considered as well. This structure type features layers of MO_6 (M = Co) octahedra. In this model, each MO_6 octahedron shares edges with six other octahedra of the same type. A fragment of the structure is shown in Figure 3c. The model performed better but still could not be refined to reproduce all details in the experimental data as the results in Figure 6c show.

Finally, the structure of the water-based nanocrystalline lithium manganese oxide was approached with that occurring in $K_xMnO_2 \cdot yH_2O$.[33] This structure type features layers of MnO_6 octahedra encapsulating K atoms and H_2O molecules. A fragment of the structure is shown in Figure 3d. This model was an excellent starting point and could be refined to reproduce very well all important details in the experimental data as shown in Figure 6d. The refined structural parameters are summarized in Table 3. The results of the structure determination carried out show that, at the atomic scale, this nanocrystalline material may well be viewed as a stack of layers made of edge-shared MnO_6 octahedra. The layers are well apart (~6.43 Å; see Figure 8a) allowing both relatively small Li and much bigger K atoms to occupy the interlayer space. This is most likely due to the aqueous preparation route employed, since it is well-known that

TABLE 3: Structural Parameters for the Hydrous K−Li−Mn−O−I Sample Obtained through PDF Analysis

a, Å	2.8317(2)
c, Å	19.29(2)
z(O)[a]	0.382(1)
U_{11}(Mn), Å^2	0.0058(1)
U_{33}(Mn), Å^2	0.148(1)
U_{iso}(Li/K/H_2O), Å^2	0.071(1)
U_{11}(O), Å^2	0.0051(1)
U_{33}(O), Å^2	0.208(1)
R_G, %	20.7

[a] The three atoms in the asymmetric unit occupy the following Wyckoff positions: Mn 3a(0,0,0); Li/K/H_2O 9d($^1/_2$,0,$^1/_2$); O 6c(0,0,*z*). Atomic positions are refined in the space group *R*3*m*. The structure is given in a hexagonal basis.

TABLE 4: Structural Parameters for Anhydrous K−Li−Mn−O−I Sample Obtained through PDF Analysis

a, Å	2.857(1)
c, Å	14.22(2)
z(O)[a]	0.233(1)
U_{11}(Mn), Å^2	0.0086(1)
U_{33}(Mn), Å^2	0.063(1)
U_{iso}(Li), Å^2	0.007(1)
U_{11}(O), Å^2	0.0064(1)
U_{33}(O), Å^2	0.154(2)
R_G, %	32.1

[a] The three atoms in the asymmetric unit occupy the following Wyckoff positions: Mn 3b(0,0,1/2); Li 3a(0,0,0); O 6c(0,0,z). Atomic positions refined in the space group $R\bar{3}m$. The structure is given in hexagonal basis.

water makes layered materials swell facilitating the encapsulation of atomic species with larger atomic radii. The layers in the nanocrystal, however, do not seem to be arranged in perfect registry. As can be seen in Table 3, the temperature factors of Mn and O atoms are highly anisotropic suggesting the presence of a significant disorder in the direction perpendicular to the layers. The disorder could be due to the presence of a distribution of interlayer distances centered at about 6.43 Å.

The search for a structure model for the anhydrous nanocrystalline sample was not so straightforward and we had to consider twice as many trial structures. The reason is that the first peak in the experimental PDF shows signatures of splitting into two subcomponents at 1.9 and ∼2.1 Å which are the lengths of Mn−O bonds in Jahn−Teller distorted octahedra (see Figure 5). This observation prompted us to explore model structures built of Jahn−Teller distorted MnO_6 octahedra at first. No signatures of Jahn−Teller distortion are seen in the hydrous sample and that is why only structures built of regular MnO_6 octahedra were considered in that case. The structural models with Jahn−Teller distorted octahedra we considered were the following: orthorhombic (space group *Pmnm*) $LiMnO_2$ (see Figure 3e); tetragonal (space group $I4_1/amd$) $Li_2Mn_2O_4$ with a distorted spinel structure (see Figure 3f); and the monoclinic (space group *C*2/*m*) layered $LiMnO_2$ structure (see Figure 3g). A comparison between the experimental and model PDFs calculated from these three structural models is shown in Figure 7, parts a−c. As can be seen, none of these models accounts well for the details of the experimental PDF. In particular, structure models involving distorted Jahn−Teller octahedra give a first PDF peak with a shoulder that is much stronger than the one experimentally observed. The observation suggests that the shoulder of the first PDF peak is likely to have some other origin. That is why the structure search was pursued further by considering models based solely on regular MnO_6 units, such as cubic $LiMn_2O_4$, monoclinic Li_2MnO_3, and rhombohedral $LiCoO_2$ (see Figure 3). Indeed, those are the structure models we already attempted with the hydrous sample. This time, however, a model based on the structure of $LiCoO_2$[34] but not $K_xMnO_2{\cdot}yH_2O$[33] performed best (see Figure 7d−f). The refined structural parameters are given in Table 4. The $LiCoO_2$-type structure model features layers of MnO_6 octahedral units encapsulating Li atoms with the interlayer separation being ∼4.7 Å only (see Figure 8b). This relatively short interlayer distance is very likely due to the fact that water was not used in the preparation; the material did not swell and thus acquired a more close packed structure. The close proximity of Mn−O layers, however, makes it possible for some Mn atoms to migrate into the interlayer Li sites and vice versa. Such substitutional disorder has been observed in crystalline layered $LiMnO_2$[2] and $LiNi_{0.4}Mn_{0.4}Co_{0.2}O_2$.[35]

We explored this possibility by allowing a partial substitution of Li atoms by Mn in our model. The best fit to the experimental PDF (shown in Figure 7f) was obtained with approximately 10% of the available interlayer Li positions occupied by Mn atoms. Interlayer Li atoms form octahedra with the oxygens from the adjacent layers and the length of Li−O bond within those octahedra is ∼2.1 Å. This coordination distance, however, is not seen in our PDF data due to the weak scattering power of Li−O atomic pairs for X-rays. However, when a small fraction (∼10%) of Li atoms is replaced by Mn, and the oxygen coordination of those interlayer atomic positions, i.e., the adjacent oxygen layers, remains more or less intact, a small-amplitude PDF feature would show up at ∼2.1 Å reflecting the Mn−O atomic pairs involving interlayer Mn atoms. Thus, according to our model, the high-r shoulder in the first peak of the experimental PDF for the anhydrous sample is due to the presence of a small number of Mn atoms in the interlayer space and not to the presence of Jahn−Teller distorted MnO_6 octahedra.

The as-refined structure with its relatively tight interlayer space, however, does not have room to accommodate K atoms that are otherwise present in the sample. It is then very likely that K forms its own, highly disordered phase that is difficult to detect by diffraction methods. An indication for the presence of an unaccounted small contribution to the experimental PDF data is the relatively high values for the agreement factor R_G = 32.1% for the anhydrous sample (compare with R_G = 20.7% for the hydrous one; see Tables 3 and 4). Other scenarios for the spatial distribution of K atoms in the anhydrous sample are also possible.

In summary, the hydrous sample refines to a single phase very well; it possesses a layered-type structure where the layers are well-separated from each other and are capable of accommodating both Li and K atoms. Even when the material is dried out and used in battery application the individual layers may remain well-separated due to the presence of interlayer K atoms that will support the layered structure as pillars. This leaves Li atoms ample space to move in and out during the charge−discharge cycles resulting in very good electrochemical performance, as observed in a recent work.[13]

On the other hand, the anhydrous sample is likely a multiphase material; it is more closely packed at the atomic scale and exhibits nonnegligible Li/Mn substitutional disorder. These structural peculiarities have an important implication on the material's performance as a battery electrode. The presence of additional phases, substitutional disorder, and the tight interlayer space would inevitably hinder the diffusion of Li and are very likely the reason for the reported poorer electrochemical performance of this material.[13]

Conclusions

Rietveld analysis and the Pair Distribution Function technique were applied successfully to study the structure of crystalline $LiMn_2O_4$ and $LiMn_{0.9}Cr_{0.1}O_2$. Both methods yield very similar structural parameters confirming the good performance of the PDF method in studying perfect crystals. The unique potential of the PDF technique to study materials of very limited structural coherence has been demonstrated by determining the atomic ordering in two nanocrystalline lithium manganese oxides. It has been found that both nanocrystals possess an atomic-scale structure very well defined on the nanometer length scale and well described in terms of symmetry, a unit cell, and a small number of atoms in it. The structure may be viewed as a stack of layers made of edge-shared MnO_6 octahedra encapsulating

K and Li atoms with the hydrous sample and Li and Mn atoms with the anhydrous sample. From the present results of our studies, the better electrochemical performance of the water-based nanocrystalline lithium manganese oxides could be attributed to their unique structure with well-separated Mn−O layers leaving Li atoms ample room to move in and out during the charge−discharge process.

Acknowledgment. Thanks are due to Mark Beno for the help with the synchrotron experiments. The work was supported by the NSF through grant DMR 0304391(NIRT) and, in part, by grant no. R08-2003-000-10409-0 from the Basic Research Program of the Korean Science & Engineering Foundation. The Advanced Photon Source is supported by the U.S. DOE under contract W-31-109-Eng-38.

References and Notes

(1) Tarascon, J.-M.; Armand, M. *Nature* **2001**, *414*, 359.
(2) Armstrong, A. R.; Bruce, P. G. *Nature* **1996**, *381*, 499.
(3) Armstrong, A. R.; Robertson, A. D.; Gitzendanner, R.; Bruce, P. G. *J. Solid State Chem.* **1999**, *145*, 549.
(4) Wills, A. S.; Raju, N. P.; Greedan, J. E. *Chem. Mater.* **1999**, *11*, 1510.
(5) Paulsen, J. M.; Thomas, C. L.; Dahn, J. R. *J. Electrochem. Soc.* **1999**, *146*, 3560.
(6) Robertson, A. D.; Armstrong, A. R.; Bruce, P. G. *Chem. Commun.* **2000**, *20*, 1997.
(7) Robertson A. D.; Bruce, P. G. *Chem. Mater.* **2003**, *15*, 1984.
(8) Shin, S.-S.; Kim, D.-W.; Sun, Y.-K. *Bull. Korean Chem. Soc.* **2002**, *23*, 679.
(9) Park, K. S.; Park, S. H.; Sun, Y.-K.; Nahm, K. S.; Yoon, C. S.; Kim, C. K.; Lee, Y. S.; Yoshio, M. *J. Electrochem. Soc.* **2002**, *149*, A1250.
(10) Jang, Y.-I.; Huang, B.; Wang, H.; Sadoway, D. R.; Chiang, Y.-M. *J. Electrochem. Soc.* **1999**, *146*, 3217.
(11) Kim, J.; Manthiram, A. *Nature* **1997**, *390*, 265.
(12) Hwang, S.-J.; Kwon, C.-W.; Portier, J.; Campet, G.; Park, H.-S.; Choy, J. H.; Huong, P. V.; Yoshimura, M.; Kakihana, M. *J. Phys. Chem. B* **2002**, *106*, 4053.
(13) Hwang, S. J.; Park, D.-H.; Kwon, C.-W.; Campet, G.; Choy, J.-H. *J. Power Sources* **2004**, *125*, 119.
(14) Sun, Y.-K.; Park, S. H.; Yoon, C. S.; Kim, C.-K.; Prakash, J. *J. Mater. Chem.* **2002**, *12*, 3827.
(15) Petkov, V.; Billinge, S. J. L.; Larson, P.; Mahanti, S. D.; Vogt, T.; K. K. Rangan, K. K.; Kanatzidis, M. G. *Phys. Rev. B* **2002**, *65*, 092105.
(16) Petkov, V.; Trikalitis, P. N.; Bozin, E. S.; Billinge, S. J. L.; Vogt, T.; Kanatzidis, M. *J. Am. Chem. Soc.* **2002**, *124*, 10157.
(17) Rietveld, H. M. *J. Appl. Crystallogr.* **1969**, *2*, 65.
(18) *The Rietveld Method*; Young, R. A., Ed.; Oxford University Press: New York, 1996.
(19) (a) Manthiram, A.; Kim, J. *Chem. Mater.* **1998**, *10*, 2895. (b) Kim, J.; Manthiram, A. *Electrochem. Solid-State Lett.* **1999**, *2*, 55.
(20) (a) Jeong, Y. U.; Manthiram, A. *Electrochem. Solid-State Lett.* **1999**, *2*, 421. (b) Jeong, Y. U.; Manthiram, A. *J. Solid State Chem.* **2001**, *156*, 331. (c) Manthiram, A.; Kim, J.; Choi, S. *MRS Symp. Proc.* **2000**, *575*, 9.
(21) Klug, H. P.; Alexander, L. E. *X-ray Diffraction Procedures for Polycrystalline Materials*; Wiley: New York, 1974.
(22) Waseda, Y. *The structure of noncrystalline materials*; McGraw-Hill: New York, 1980.
(23) Petkov, V.; Jeong, I.-K.; Chung, J. S.; Thorpe, M. F.; Kycia, S.; Billinge, S. J. L. *Phys. Rev. Lett.* **1999**, *83*, 4089.
(24) Petkov, V. *J. Appl. Crystallogr.* **1989**, *22*, 387.
(25) Izumi, F.; Ikeda, T. *Mater. Sci. Forum* **2000**, *321−324*, 198.
(26) Larson, A. C.; Von Dreele, R. B. *Los Alamos National Laboratory Report*, LAUR 86-748, 2000.
(27) Rodríguez-Carvajal, J. *Physica B* **1993**, *192*, 55.
(28) Sigala, C.; Verbaere, A.; Mansot, J. L.; Guyomard, D.; Piffard, Y.; Tournoux, M. *J. Solid State Chem.* **1997**, *132*, 372.
(29) Hwang, S.-J.; Park, H.-S.; Choy, J.-H.; Campet, G. *J. Phys. Chem. B* **2000**, *104*, 7612.
(30) Proffen, Th.; Billinge, S. J. L. *J. Appl. Crystallogr.* **1999**, *32*, 572.
(31) Jeong, I.-K.; Proffen, Th.; Mohiuddin-Jacobs, F.; Billinge, S. J. L. *J. Phys. Chem. A* **1999**, *103*, 921.
(32) Petkov, V.; Zavalij, P. Y.; Lutta, S.; Whittingham, M. S.; Parvanov, V.; Shastri, S. *Phys. Rev. B* **2004**, *69*, 085410.
(33) Chen, R.; Zavalij, P.; Whittingham, M. S. *Chem. Mater.* **1996**, *8*, 1275. According to a private communication from the authors, the correct fractional coordinates for the oxygen atoms in Table 2 are 0, 0, 0.372(3).
(34) Holzapfel, M.; Haak, C.; Ott, A. *J. Solid State Chem.* **2001**, *156*, 470.
(35) Ngala, J. K.; Chernova, N. A.; Ma. M.; Mamak, M.; Zavalij, P. Y.; Whittingham, M. S. *J. Mater. Chem.* **2004**, *14*, 214.